American Meteorological Society
11th Conf. on Mountain Meteorology
21-25 June 2004, Bartlett NH, USA

8.3 NOCTURNAL BOUNDARY LAYER COOLING RATES IN VALLEYS, BASINS, AND OVER PLAINS

Stephan F. J. De Wekker* and C. David Whiteman
Pacific Northwest National Laboratory, Richland, Washington

1. INTRODUCTION

The boundary layer warms up during daytime and cools down during nighttime in response to the changing available energy at the earth's surface. Around sunset when the available energy becomes negative, temperatures start to fall and a stable or nocturnal boundary layer forms. The boundary layer continues to cool during the night, leading to a temperature minimum near sunrise. Because good forecasts of minimum temperatures have an important practical value that extends to fog and frost predictions, a number of investigators have attempted to model the nocturnal cooling. A simplified analytical model developed by Brunt (1939) and later extended by Groen (1947) predicts the decrease in surface temperature using a balance between net radiative loss at the surface and ground heat flux. The model predicts that surface temperatures will decrease with the square root of time. Brunt (1939) compared the theoretical prediction with observations of surface temperature and found good correspondence. In contrast, a recent study by Pattantyús-Abrahám and Jánosi (2004) show a better fit of screen-level temperature observations with an exponential function. Surridge (1986) extended consideration to the vertical temperature difference between the surface and the top of the boundary layer, providing a theoretical basis that predicts that the temperature difference or inversion strength increases with the square root of time. Surridge and Swanepoel (1987) show that observed temperature differences are initially faster than the predicted square root dependence and may be more appropriately described by an error function.

The major processes determining the rate of change of temperature in the boundary layer are advection and turbulent and radiative heat flux divergences. The importance of radiative flux divergence in the initial rapid cooling phase of the nocturnal boundary layer has been shown in various studies (e.g., André and Mahrt 1982; Sun et al. 2003). Topography can affect the cooling in various ways. In valleys, cooling rates during clear, undisturbed nighttime periods are affected by the presence of thermally driven slope and valley winds. Early in the evening, downslope flows develop along the sidewalls because radiative cooling at the sidewall surface and subsequent downward turbulent transfer of heat causes the layer of air adjacent to the slope to be colder than air at the same level away from the slope. The cold air flowing down the slope converges over the valley floor, building up the inversion depth over time, and resulting in inversions in valleys that are usually deeper than those over adjacent flat terrain areas. The evening and nighttime down-slope flows that produce the convergence are usually accompanied by down-valley flows that carry the air cooled within the valley out the valley exit onto the adjacent plain. The cold air carried down the valley is replaced by potentially warmer air that subsides into the valley from aloft. This warm air decelerates the cooling which, in turn, reduces the along-valley pressure gradient and the intensity of the valley wind system (Whiteman 2000). The complex interactions between advection and turbulent and radiative heat flux divergence makes the theoretical prediction of nighttime cooling rates very difficult. In perfectly closed basins, the complexity is reduced because horizontal advection is absent. Whiteman and Haiden (2004, this issue) show that in these cases the total cooling on the basin floor may be primarily a function of the sky-view factor.

It is not known to what extent cooling rates differ in various types of topography and whether certain topographic forms (e.g., valleys, basins and plains) have characteristic cooling rates. The identification of characteristic types of cooling profiles in the different topographic settings might prove useful for predicting nocturnal minimum temperatures or for identifying and quantifying different cooling mechanisms. In the current paper, we use existing data to explore atmospheric cooling rates in a variety of valley, basin and plains atmospheres under undisturbed, clear-sky conditions. The previous studies, referenced above, have restricted consideration to surface temperatures, or temperature differences between the surface and the top of the nocturnal boundary layer over homogeneous terrain. Because surface temperatures are often very sensitive to local conditions in complex terrain, we take the approach of investigating the vertically and horizontally integrated cooling throughout the entire valley or basin volume up to the top of the nocturnal boundary layer. This approach requires detailed vertical temperature sounding data but reduces the sensitivity of the calculations to surface microclimates and to uncertainties in the determination of nocturnal boundary layer depths.

2. APPROACH

By integrating the potential temperature tendency $\partial\theta / \partial t$ over time t and height z from the surface to a given height h we obtain the cumulative atmospheric heat storage per unit area

Corresponding author address: Stephan F. J. De Wekker, PNNL, P.O. Box 999, Richland, WA 99352 email: stephan.dewekker@pnl.gov

$$H(t) = \int_0^h c_p \rho(t,z)\, \Delta\theta(t,z)\, dz \qquad [\text{J m}^{-2}] \qquad (1)$$

where c_p is the specific heat of air at constant pressure, $\rho(t,z)$ is the air density, and $\Delta\theta(t,z) = \theta(t,z) - \theta(t_0)$ is the temperature difference between a given vertical profile of potential temperature at time t and a neutral potential temperature profile at an initial time t_0. The height h corresponds to the height of the nocturnal inversion at around sunrise when this layer is deepest.

To compare the accumulated cooling in valleys and basins of different size, we need to multiply the term within the integral of (1) by the factor $A(z)/A_h$ where $A(z)$ and A_h are the valley or basin drainage areas at height z and at height h, respectively. This way, we obtain the 'topography-weighted' cumulative heat storage

$$S(t) = \int_0^h c_p \rho(t,z)\, \Delta\theta(t,z)\, \frac{A(z)}{A_h}\, dz \qquad [\text{J m}^{-2}]. \qquad (2)$$

For the evaluation of $S(t)$ in a valley or basin we assume that $\Delta\theta(t,z)$ is homogeneous from sidewall to sidewall. Note that Eq. 2 can also be used for flat terrain if A is taken to be invariant with height.

In this paper, we calculate $H(t)$ for a broad variety of valleys and basins using sequences of vertical tethersonde soundings over valley or basin centers from around sunset to around sunrise. The height of the nocturnal inversion h is taken as the height where a significant change in $d\theta/dz$ occurred on near-sunrise soundings. For the calculation of $S(t)$ in basins, $A(z)$ was determined from topographic maps and a planimeter. For valleys, $S(t)$ was determined for a unit-long valley segment from estimates of the valley width and slope angles, and $A(z)$ is the valley width times the 1-m length of the valley segment.

The initial time t_0 was taken as the latest time of the day when the potential temperature profile was approximately neutral. This was usually about an hour before astronomical sunset. However, in snow-covered wintertime cases when the inversion persisted during the entire day and no neutral profile was observed, time t_0 was taken as the time of the sounding nearest sunset. The final time in all cases was taken as the coldest sounding in the sequence, usually corresponding to a time near sunrise. To calculate $H(t)$ from individual soundings, balloon data were first interpolated to regular height intervals. As mentioned before, the integration height was chosen based on the inversion height near sunrise. If the near-sunrise sounding did not reach this height, the soundings were extended to the integration height by interpolation from previous and subsequent soundings.

3. DATA

The experimental approach has been applied to series of tethered balloon temperature soundings from valleys and basins of different sizes and shapes, as well as those over flat plains. The data chosen for analysis were collected in high pressure weather with clear skies and weak upper level winds, as these are the conditions that generally lead to the strongest inversions and cooling rates. The soundings were collected over the course of entire nights, but usually with the highest sounding frequency in the early- to mid-evening. A near-sunrise sounding was required to meet the requirements of the experimental approach, and soundings had to be of sufficient depth to include the entire inversion layer. Data were available from a range of different valley, basin and plains sites in different seasons, as shown in Table 1, which also lists the topographic characteristics of the sites. The accompanying Table 2 provides selected analysis results.

4. RESULTS

4.1 Cooling of the Stable Boundary Layer over Valleys, Plains and Basins

The cumulative cooling of the stable boundary layer was calculated from series of tethersonde ascents using Eq. 1 and 2. The cumulative cooling was then normalized by dividing $H(t)$ and $S(t)$ by the total accumulated nighttime cooling at (or near) sunrise, H_T and S_T, respectively. H_T and S_T are calculated from Eq. 1 and 2 by setting $\Delta\theta(t,z) = \theta(t_{SR},z) - \theta(t_0)$, where $\theta(t_{SR},z)$ is the near-sunrise temperature sounding. The normalized total accumulated nighttime cooling values H/H_T and S/S_T were then plotted as a function of elapsed time $t - t_0$ (time since neutral profile) and were fit by three different functions, an exponential function,

$$\frac{H}{H_T} = 1 - \exp\left(-\frac{t-t_0}{\tau_{\exp}}\right), \qquad (3)$$

an error function,

$$\frac{H}{H_T} = erf\left(\frac{t-t_0}{\tau}\right), \qquad (4)$$

and a square root function,

$$\frac{H}{H_T} = C\sqrt{t-t_0} \qquad (5)$$

where $\tau_{\exp}$ and τ are the fitting parameters for the exponential and the error functions respectively, and C is a constant. The fitting parameters characterize the

Table 1. Valleys, measurement sites, dates and topographic characteristics.

Location	Nr.	Date	Lat. (°)	Long. (°)	Valley Depth (m)	Valley Width (m)	Sidewall Angles (deg)	Drainage Area (km^2)	Length of Night (h)
Peter Sinks Basin, Utah	1	09/08-09/1999	41.915 N	111.511 W	120	--	--	2.25	11.18
Gruenloch Basin, Austria	2	06/02-03/2002	47.821 N	15.045 E	120	--	--	1.82	8.23
Sinbad Basin, Colorado	3	07/15-16/1988	38.514 N	108.987 W	--	--	--	83.82	9.55
S Fk White R. Valley, Colo.									
River Cabin	4	08/24-25/1978	39.974 N	107.625 W	300	a)	a)	448	10.6
River Cabin	5	08/28-29/1978	39.974 N	107.625 W	300	a)	a)	448	10.77
Mobley's Y-Z Ranch	6	08/27-28/1978	39.955 N	107.584 W	350	400	18, 15	421	10.72
Mobley's Y-Z Ranch	7	08/28-29/1978	39.955 N	107.584 W	350	400	18, 15	421	10.77
Yampa Valley, Colorado									
Sombrero Ranch	8	02/04-05/1978	40.458 N	106.814 W	450	2580	16, 09	1370	13.72
Sombrero Ranch	9	02/23-24/1978	40.458 N	106.814 W	450	2580	16, 09	1370	12.97
Horseshoeing School	10	08/09-10/1978	40.450 N	106.814 W	450	2580	16, 09	1370	10.05
Eagle Valley, Colorado									
Ray Millers Ranch	11	10/13-14/1977	39.641 N	106.571 W	700	1450	21, 10	1061	12.73
Gore Valley, Colorado									
Vail Safeway	12	12/09-10/1975	39.631 N	106.418 W	600	390	15, 16	233	14.92
Kansas (CASES-99)	13	10/10-11/1999	37.65 N	96.73 W	--	--	--	--	12.55
Wangara, Australia	14-18	July 1967 (5)	34.5 S	144.93 E	--	--	--	--	13.9

a) Valley width and sidewall angles could not be determined in this valley due to terrain complexity.

Table 2: Stable boundary layer characteristics.

Location	Integration (inversion) Depth (m)	inversion Strength (°C) at Sunrise	Maximum Accumulated Cooling (MJ m^{-2})	Maximum Accumulated Cooling (topo-weighted)	τ_{exp} (h)	τ_{erf} (h)
Peter Sinks Basin, Utah	150	22	2.0	1.0	3.1	3.1
Gruenloch Basin, Austria	100	12	1.1	0.4	3.2	3.1
Sinbad Basin, Colorado	550	15	5.2	2.0	5.4	5.4
S Fk White R. Valley, Colorado						
River Cabin	400	12	6.0	n/a	3.9	3.6
River Cabin	550	18	6.1	n/a	4.6	4.2
Mobley's Y-Z Ranch	550	14	8.1	3.7	5.5	5.4
Mobley's Y-Z Ranch	500	16	6.2	2.8	5.1	4.6
Yampa Valley, Colorado						
Sombrero Ranch	520	27	3.2	1.7	5.2	4.7
Sombrero Ranch	550	25	5.3	3.0	7.5	7.5
Horseshoeing School	600	17.5	6.0	3.0	4.4	4.7
Eagle Valley, Colorado						
Ray Millers Ranch	510	15.5	9.7	5.4	6.4	5.8
Gore Valley, Colorado						
Vail Safeway	450	17	4.3	2.0	4.3	4.2
Kansas (CASES-99)	120	10	1.0	n/a	5.8	5.8
Wangara, Australia (5 cases avg)	310	9.5	2.1	n/a	5.3	5.5

rate of cooling of the valley atmosphere, where τ_{exp} and τ are the times required for the cumulative cooling to attain 63.2% and 84.3% of its total nighttime value, respectively. For ease in comparing the exponential and error function fits, we report the 63.2% (i.e., $1-1/e$) time constants for both functions using the symbols τ_{exp} and τ_{erf}.

The procedure described above is shown for selected basin, valley and plains sites in Fig. 1. The square root fit clearly over-predicts cooling rates at all locations in the first few hours of the night, while both the error and exponential functions provide suitable approximations to the data. The error function provided a better fit to the cumulative cooling rates in the second half of the night, and gave more favorable chi-squared values compared to the exponential fit.

Fits were obtained for all the sites and dates listed in Table 1. The computed time constants τ_{exp} and τ_{erf} along with the integration depths, the inversion strengths at sunrise, and the maximum accumulated cooling calculated with and without topography weighting are provided in Table 2. Because normalization tends to make the H/H_T and S/S_T curves nearly coincident, we will focus our discussions entirely on the non-topography-weighted curves and calculations.

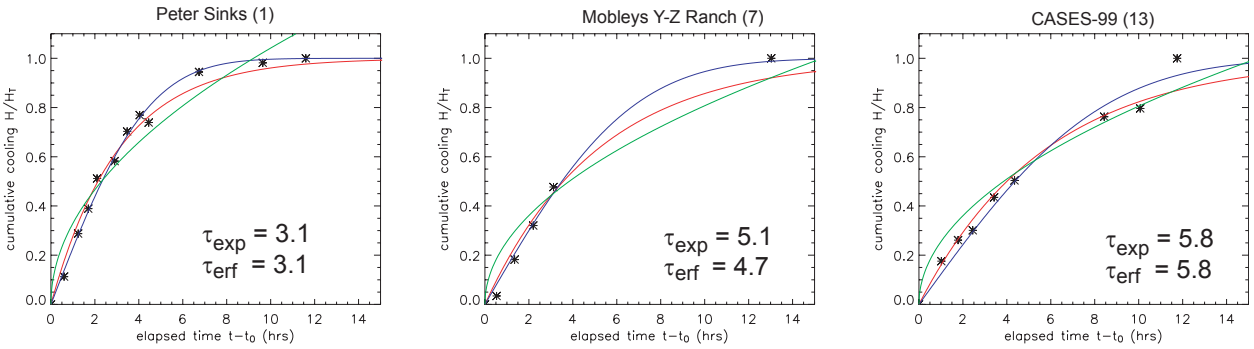

Figure 1. Normalized cumulative cooling H/H_T as a function of elapsed time $t-t_0$ for 3 basin (Peter Sinks), valley (Mobley Y-Z Ranch) and plain (CASES-99) sites. Red, blue, and green lines are the exponential, error function, and square root fits to the data (stars). τ_{exp} and τ_{erf} are the time constants for the exponential and error function fits, respectively. The numbers in parentheses on top of each subfigure correspond to the station numbers in Table 1, where additional information on the terrain can be found.

Since the error function curve provides a good fit to most of the data, we illustrate this fit for a selected set of valleys, basins and plains in Fig. 2. As expected, the basin atmospheres cool the fastest with τ_{erf} = 3.1 hours (Fig. 2a), while typical values in flat terrain are around 5-6 hours (Fig. 2d). The 4.2 to 5.4 hour time constants for the White River and Yampa Valleys (Figs. 2b,c) are intermediate between those of the small closed basins and the plains. Data from various locations inside the White River Valley (Fig. 2c) on different days show a rather narrow range of time constants from 3.6 to 5.4 hours. Time constants can be much longer in snow-covered valleys when the previous night's inversion is still present at the beginning of the evening transition period. The normally high rates of cooling associated with the evening transition period are greatly suppressed in this case. This is illustrated by the snow-covered Yampa Valley (Fig. 2c, case 9), which had a time constant of 7.5 hours.

The results of the time constant analysis for all of the locations and dates (Table 1) that were investigated is shown in Fig. 3, where the error function time constant is plotted as a function of accumulated nighttime cooling. The total nighttime cooling varies significantly from site to site. The inversions that form in the small Peter Sinks and Gruenloch basins (sites 1 and 2) are quite shallow, as are the inversions that form over plains (13 and 14). Because their inversions are shallow, these sites experience small cumulative heat losses relative to the deeper valleys. A similarly broad range of time constants is also apparent among the sites, with the basins having the smallest time constants, the plains having the largest time constants, and the valleys having time constants that are intermediate in value. The Sinbad Basin is an apparent exception to the rule that basins will have short time constants. Investigations of the meteorology of this basin (Whiteman et al. 1996), however, have shown that the Sinbad Basin has a strong down-valley flow that occurs through a narrow drainage canyon and is thus more like a valley than a basin.

Even though we have a large selection of cases that show that cumulative cooling exhibits an exponential or error function dependency, we are not able to make any conclusive statements whether a certain basin or valley location has a 'typical' time constant. It does, however, not seem likely given the many processes affecting cooling rates and the interaction between them. We could also not detect any clear dependency of the time constant on valley geometry or boundary layer characteristics such as inversion height and strength (Tables 1 and 2). Surface characteristics and ambient atmospheric conditions probably play an important role. For example, a variation in valley flow characteristics between different cases will affect the significance of the subsidence warming mechanism outlined in the introduction. An analysis of mean wind speeds during the night in the various valleys, however, indicated that the time constant is insensitive to the mean wind speed.

4.2 Variation of Cooling Rates with Altitude on Basin Sidewalls

In section 4.1 we calculated the cumulative cooling and time constants in atmospheric *volumes* enclosed in valleys or basins or in nocturnal stable boundary layers over plains. Earlier investigators (e.g., Pattantyús-Abrahám and Jánosi 2004) computed cooling time constants for near-surface point temperature measurements over flat plains rather than for

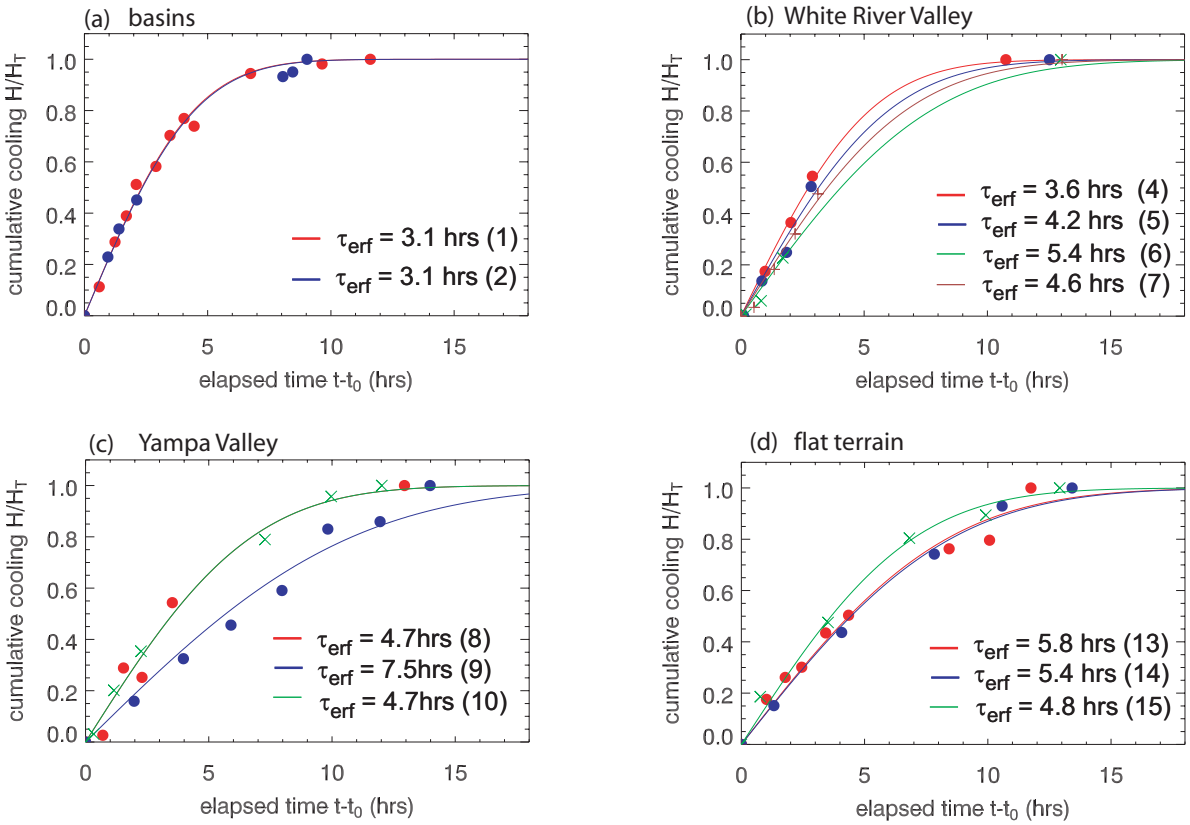

Figure 2. Normalized cumulative cooling H/H_T as a function of elapsed time $t-t_0$ for (a) basin, (b) White River Valley, (c) Yampa Valley, and (d) flat terrain sites. The colored lines are fits to data points of the same color. The time constants τ_{erf} are also indicated. The numbers in parentheses correspond to the station numbers in Table 1.

atmospheric volumes. In this section, we make time constant calculations from two lines of surface-based temperature data loggers exposed at 1.4 m AGL and running up the northwest and southeast sidewalls of the Gruenloch Basin (Whiteman et al. 2004). We then compare the time constants for the point measurements at different altitudes with the time constant calculated for the same date for the atmospheric volume enclosed within the basin to gain insight into the cooling mechanisms. Interpretation of the results requires knowledge of the topographic characteristics of the Gruenloch Basin. The basin is fully enclosed by topography from the basin floor (1270 m MSL) to the lowest saddle (1324 m MSL). Above the saddle, the basin is unconfined and air cooled within the upper basin is known to flow out of the basin through the gap above this saddle. Typical inversion depths are about 120 m above the floor (1390 m MSL). An example of the cooling curves and exponential function fits to the curves for 5 selected sites from the northwest line of data loggers is shown in Fig. 4. The exponential function used to fit the data was

$$T(t) = [T_0 - T_c]\exp\left(-\frac{t-t_0}{\tau_{\exp}}\right) + T_c \qquad (6)$$

where T_0 is the temperature at initial time t_0 (we use the same t_0 as in the calculation of $H(t)$) and T_c is the asymptotic cooling temperature. This function fit the observations well.

The approach illustrated in Fig. 4 was modified slightly to allow comparisons between the two lines of data loggers in the Gruenloch Basin. Because of the effects of shadows and the exposure to the setting sun, the starting times for the evening transition cooling differed between the two sidewalls. To put the analyses on the same basis we selected the time interval between 1900 and 0405 Central European Standard Time (CEST) for the time constant calculations. The 1900 CEST starting time was chosen because cooling was occurring on both sidewalls by this time, and the 0405 CEST ending time is the approximate time of sunrise. Astronomical sunset was at 1946 CEST.

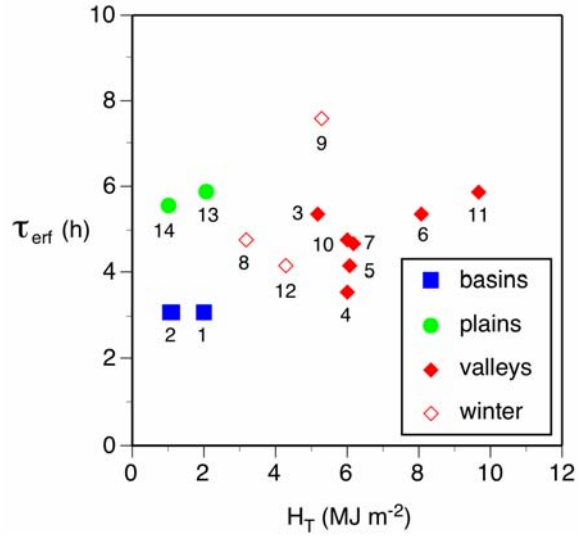

Figure 3. Time constant (in hours) as a function of accumulated nighttime cooling for basins, valleys and plains. The valley points include both snow-covered (hollow diamonds) and non-snow-covered (solid diamonds) valleys. The numbers correspond to the station numbers in Table 1.

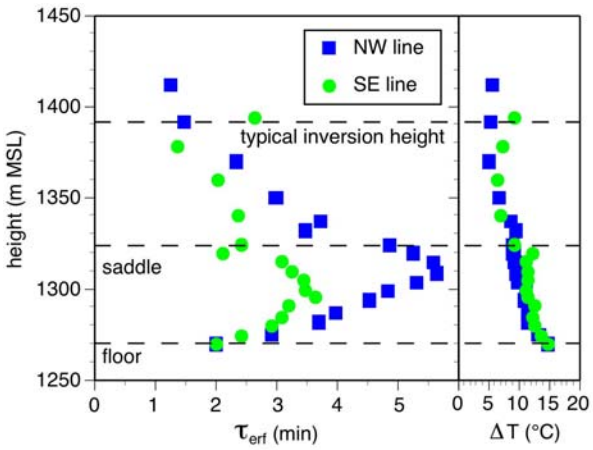

Figure 5. Time constant and temperature drop from 1900 to 0405 CEST as a function of height for temperatures at 1.4 m AGL on lines running up the northwest and southeast sidewalls of Austria's Gruenloch Basin on 2-3 June 2002. The horizontal dashed lines denote the height of the basin floor, the lowest saddle (Lechner Saddle) and the typical temperature inversion top.

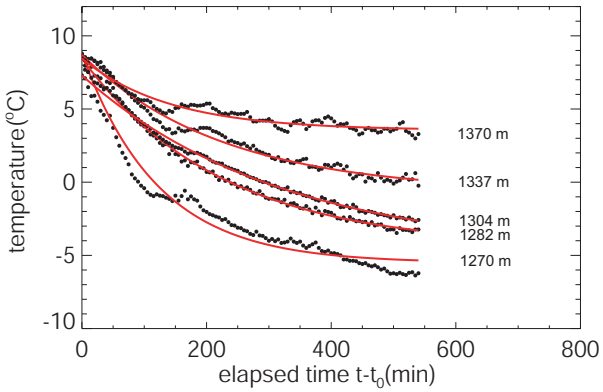

Figure 4. Observed surface temperatures in the Gruenloch Basin at five different elevations as a function of elapsed time $t - t_0$ (the time since the onset of a stable atmosphere in the basin). The red lines are best fit exponential curves.

The variation with height of the time constants τ_{erf} and the drops in temperature ΔT during the selected time interval at the two lines of surface stations are depicted in Fig. 5. The temperature drop is highest at the basin floor (~15°C) and decreases with height to attain about 5°C at and above the saddle. The drop during the time interval of interest is higher on the southeast sidewall than on the northwest sidewall, since the southeast sidewall is illuminated more directly by the setting sun. Whiteman et al. (2004) show that the air temperatures in the Gruenloch Basin rapidly become equilibrated between the sidewalls after sunset. The air enclosed in the basin below the saddle cools much more strongly than the air above the saddle because warmer air from aloft subsides into the upper basin as cold air drains through the gap above the saddle. These processes are the cause of the rather sharp discontinuity in temperature drop at the altitude of the saddle on the southeast line and about 20 m above the saddle on the northwest line.

Time constants at the surface stations fall in the range from 1 to 6 hours. They are shortest or, equivalently, cooling rates are largest, near the basin floor and above the saddle. The short time constants on the upper sidewalls compared to the lower enclosed basin are consistent with large net longwave radiative losses on the upper sidewalls. Net radiative losses on the lower sidewalls are reduced by back-radiation from the surrounding sidewalls. These radiative effects cannot explain the short time constant at the basin floor, but the rapid cooling there may be caused by a transient cold air drainage that occurs in the early evening. The maximum time constants are found in the upper part of the enclosed basin below the saddle where neither the radiative losses nor the accumulation of cold air by drainage are effective in producing local cooling. The shapes of the time constant profiles are similar on the two sidewalls, but time constants are smaller (i.e., cooling rates are higher) on the southeast line than on the northwest line. This would be consistent with larger longwave radiative losses from the warmer southeast sidewall. The shapes of the time constant profiles was not sensitive to the choice of different starting times,

and the basic features of the time constant profiles were also observed for the following night of 3-4 June 2002.

The volumetric and point time constants for the basin atmosphere and sidewalls can be compared. The time constant for the cooling of the basin atmospheric volume (Table 2) was 3.1 hours. This volumetric time constant is roughly the average of the time constants from the point measurements on the sidewalls enclosing the volume, suggesting that basin atmosphere simply integrates the cooling rates observed on the surrounding sidewalls.

5. CONCLUSIONS

The volumetric cumulative cooling in nighttime stable boundary layers that form in valleys and basins and over flat terrain on clear, undisturbed nights increases with time following an exponential or error function shape rather than a square root shape. The cooling rates vary significantly among the individual valley, basin and plains locations chosen for the analysis. An error function or exponential fit to the observed accumulated cooling curves allowed us to calculate a volumetric time constant or nocturnal cooling time scale. The time constants are in the range from 3 to 6 hours, indicating that 62.5% of the cumulative nocturnal cooling occurs over this time interval. We do not have enough data from multiple nights in the same valley or basin locations to determine whether a cooling time constant might be a useful parameter describing individual valleys or basins. Such a parameter might be useful, for example, in predicting minimum temperatures. The calculated time constants were shortest in small enclosed basins, longest in nocturnal boundary layers that form over plains, and intermediate in valleys. The time constants can be quite long in snow-covered valleys where inversions may persist for multiple days.

An analysis of point temperature data from multiple locations on the sidewalls of the Gruenloch Basin revealed that the cooling time constants for point locations are altitude-dependent, and vary within the range from 1 to 6 hours. The shortest time constants (i.e., maximum rates of cooling) were found in the upper basin above the lowest saddle and at the basin floor. The maximum time constant occurred below the saddle in the upper part of the fully enclosed lower basin. Preliminary hypotheses have been presented to relate these variations in cooling rates to radiative transfer and air drainage effects.

In our future analysis, we will explore further the data sets we have available and utilize numerical models to investigate the factors affecting cooling rates near the surface and in the boundary layer. For example, we would like to investigate how the intensity of the valley flow affects cooling rates and time constants and if 'typical' time constants can be defined for valleys of different sizes.

Acknowledgments

Research support was provided by the U.S. Department of Energy's (DOE) Vertical Transport and Mixing (VTMX) program under the auspices of the Environmental Meteorology Program of the Office of Biological and Environmental Research. The research was conducted at Pacific Northwest National Laboratory, which is operated for DOE by Battelle Memorial Institute.

References

André, J.-C., and L. Mahrt, 1982: The nocturnal surface inversion and influence of clear-air radiative cooling. Temporal and spatial variability. *J. Atmos. Sci.*, **58**, 2650-2667.

Brunt, D., 1939: *Physical and dynamical meteorology, 2nd Ed*. Cambridge Univ. Press, Cambridge, 428 pp.

Clements, C. B., C. D. Whiteman, and J. D. Horel, 2003: Cold-air-pool structure and evolution in a mountain basin: Peter Sinks, Utah. *J. Appl. Meteor.*, **42**, 752-768.

Groen, P., 1947: Note on the theory of nocturnal radiational cooling of the earth's surface. *J. Meteor.*, **4**, 63-66.

Mahrt, L., 1999: Stratified atmospheric boundary layers. *Bound.-Layer Meteor.*, **90**, 375-396.

Pattantyús-Abrahám, M., and I.M. Jánosi, 2004: What determines the nocturnal cooling timescale at 2 m? *Geophys. Res. Letters*, **31**, L05109, doi:10.1029/2003GL019137.

Sun, J., S. P. Burns, A. C. Delany, S. P. Oncley, T. W. Horst, and D. H. Lenschow, 2003: Heat balance in the nocturnal boundary layer during CASES-99. *J. Appl. Meteor.,* **42**, 1649-1666.

Surridge, A.D., 1986: The evolution of the nocturnal temperature inversion. *Bound.-Layer Meteor.*, **36**, 295-305.

_____, and D. J. Swanepoel, 1987: On the evolution of the height and temperature difference across the nocturnal stable boundary layer. *Bound.-Layer Meteor.*, **40**, 87-98.

Whiteman, C. D., 2000: *Mountain Meteorology: Fundamentals and Applications*. Oxford University Press, New York, 355pp.

_____, and T. Haiden, 2004: Processes leading to inversion buildup in small enclosed basins. In: Proceedings, 11th Conf. on Mountain Meteor., 21-25 June 2004, Bartlett, NH, USA.

_____, T. B. McKee, and J. C. Doran, 1996: Boundary layer evolution within a canyonland basin. Part I. Mass, heat, and moisture budgets from observations. *J. Appl. Meteor.*, **35**, 2145-2161.

_____, S. Eisenbach, B. Pospichal, and R. Steinacker, 2004: Comparison of vertical soundings and sidewall air temperature measurements in a small Alpine basin. Submitted to *J. Appl. Meteor*.